J|A|C|S
ARTICLES
Published on Web 05/19/2007

Nanosize Effect on High-Rate Li-Ion Intercalation in $LiCoO_2$ Electrode

Masashi Okubo,[†,⊥] Eiji Hosono,[†] Jedeok Kim,[‡] Masaya Enomoto,[§] Norimichi Kojima,[§] Tetsuichi Kudo,[†] Haoshen Zhou,[†] and Itaru Honma*[,†]

Contribution from the National Institute of Advanced Industrial Science and Technology (AIST), Umezono, 1-1-1, Tsukuba, Ibaraki 305-0012, Japan, National Institute for Materials Science (NIMS), Tsukuba, Ibaraki 305-0044, Japan, and Graduate School of Arts and Sciences, the University of Tokyo, Meguro-ku, Tokyo 153-8902, Japan

Received November 15, 2006; E-mail: i.homma@aist.go.jp

Abstract: Recently, battery technology has come to require a higher rate capability. The main difficulty in high-rate charge−discharge experiments is kinetic problems due to the slow diffusion of Li-ions in electrodes. Nanosizing is a popular way to achieve a higher surface area and shorter Li-ion diffusion length for fast diffusion. However, while various nanoelectrodes that provide excellent high-rate capability have been synthesized, a size-controlled synthesis and a systematic study of nanocrystalline $LiCoO_2$ have not been carried out because of the difficulty in controlling the size. We have established the size-controlled synthesis of nanocrystalline $LiCoO_2$ through a hydrothermal reaction and, for the first time, clarified the structural and electrochemical properties of this intercalation cathode material. Lattice expansion in nanocrystalline $LiCoO_2$ was found from powder X-ray diffraction measurements and Raman spectroscopy. Electrochemical measurements and theoretical analyses on nanocrystalline $LiCoO_2$ revealed that extreme size reduction below 15 nm was not favorable for most applications. An excellent high-rate capability (65% of the 1 C rate capability at 100 C) was observed in nanocrystalline $LiCoO_2$ with an appropriate particle size of 17 nm.

Introduction

Li-ion rechargeable batteries are widely used for consumer electronic devices, like cellular phones and portable computers. Although, their high voltage, portability, and excellent cyclability have contributed to the commercial success of Li-ion rechargeable batteries, new applications, like hybrid electric vehicles, require a higher charge−discharge rate capability. For the higher rate capability, we should tackle a kinetic problem due to the slow diffusion of Li-ions in electrodes.

To use nanoelectrodes is one of the effective ways to overcome this problem. Their higher surface area and shorter Li-ion diffusion length due to small particle size should contribute to the higher-rate capability. In this context, various nanoelectrodes that have a high-rate capability have been synthesized.[1−5] For example, the lithium-ion diffusion coefficient, D_{Li}, in cathode material $LiCoO_2$ was estimated at $10^{-11.6}$ cm^2/s from electrochemical impedance spectroscopy.[6] Based on this value, a discharge process (intercalation of lithium-ions) of 1 s requires a lithium-ion diffusion length of below 15 nm, i.e., a particle size below 30 nm. While many groups have reported nanocrystalline $LiCoO_2$ synthesized through a post-templating method,[7] a sol−gel method,[8,9] a spray-drying method,[10] a coprecipitation method,[11] and a hydrothermal method,[12−15] a precisely size-controlled synthesis and a systematic study of nanocrystalline $LiCoO_2$ have not been carried out because of the difficulties in controlling the size. In this article, we describe the systematic synthesis of nanocrystalline $LiCoO_2$, which could be widely applicable to the systematic synthesis of other cathode nanoparticles, and present the first complete study on its structural and electrochemical properties.

† National Institute of Advanced Industrial Science and Technology.
‡ National Institute for Materials Science.
§ The University of Tokyo.
⊥ Present address: Department of Applied Chemistry, Faculty of Science and Engineering, Chuo University, Kasuga 1-13-27, Bunkyo-ku, Tokyo 112-8551, Japan.

(1) Poizot, P.; Laruelle, S.; Grugeon, S.; Dupont, L.; Tarascon, J.−M. *Nature* **2000**, *407*, 496.
(2) Larcher, D.; Masquelier, C.; Bonnin, D.; Chabre, Y.; Masson, V.; Leriche, J.-B.; Tarascon, J.-M. *J. Electrochem. Soc.* **2003**, *150*, A133.
(3) Armstrong, A. R.; Armstrong, G.; Canales, Garcia, J. R.; Bruce, P. G. *Adv. Mater.* **2005**, *17*, 862.
(4) Sides, C. R.; Li, N. C.; Patrissi, C. J.; Scrosati, B.; Martin, C. R. *Mater. Res. Bull.* **2002**, *27*, 604.
(5) Arico, A. S.; Bruce, P.; Tarascon, J.-M.; Schalkwijk, W. V. *Nature Mater.* **2005**, *4*, 366.
(6) Levi, M. D.; Salitra, G.; Markovsky, B.; Teller, H.; Aurbach, D.; Heider, U.; Heider, L. *J. Electrochem. Soc.* **1999**, *146*, 1279.
(7) Jiao, F.; Shaju, K. M.; Bruce, P. G. *Angew. Chem. Int. Ed.* **2005**, *44*, 6550.
(8) Peng, Z. S.; Wan, C. R.; Jiang, C. Y. *J. Power Sources* **1998**, *72*, 215.
(9) Yoon, W. S.; Kim, K. B. *J. Power Sources* **1999**, *81*−*82*, 517.
(10) Li, Y.; Wan, C.; Wu, Y.; Jiang, C.; Zhu, Y. *J. Power Sources* **2000**, *85*, 294.
(11) Chen, H.; Qiu, X.; Zhu, W.; Hagenmuller, P. *Electrochem. Commun.* **2002**, *4*, 488.
(12) Larcher, D.; Palacin, M. R.; Amatucci, G. G.; Tarascon, J.-M. *J. Electrochem. Soc.* **1997**, *144*, 408.
(13) Tabuchi, M.; Ado, K.; Kobayashi, H.; Sakaebe, H.; Kageyama, H.; Masquelier, C.; Yonemura, M.; Hirano, A.; Kanno, R. *J. Mater. Chem.* **1999**, *9*, 199.
(14) Kobayashi, H.; Shigemura, H.; Tabuchi, M.; Sakaebe, H.; Ado, K.; Kageyama, H.; Hirano, A.; Kanno, R.; Wakita, M.; Morimoto, S.; Nasu, S. *J. Electrochem. Soc.* **2000**, *147*, 960.
(15) Burukhin, A.; Brylev, O.; Hany, P.; Churagulov, B. R. *Solid State Ionics* **2002**, *151*, 259.

 10.1021/ja0681927 CCC: $37.00

Table 1. Selected Synthetic Conditions and Obtained Products

reaction temp (°C)	reaction time (h)	[LiOH] (mol/L)	crystallite size (thickness) (nm)	phase composition	*c*/*a*
170	12	0.1	27	$LiCoO_2$	4.9917
170	12	1	17	$LiCoO_2$	4.9816
170	12	5	11	$LiCoO_2$	5.0057
150	12	0.1	32	$LiCoO_2$	4.9798
150	12	1	11	$LiCoO_2$	4.9849
150	12	5	9	$LiCoO_2$	4.9959
120	12	1	−	CoOOH	−
120	12	5	7.4	$LiCoO_2$	5.0026
120	9	5	6	$LiCoO_2$	5.0048
120	6	5	5.7	$LiCoO_2$	4.9938
100	12	5	−	CoOOH	−

Experimental Section

All reagents and bulk $LiCoO_2$ were purchased commercially. CoOOH with a thickness of 8 nm was synthesized by using an air oxidation method.[16] A dilute aqueous solution (100 mL) of $Co(NO_3)_2 \cdot 6H_2O$ (5.82 g, 0.02 mol) was slowly added to 100 mL of an aqueous 5 M NaOH solution. The resulting pink $Co(OH)_2$ suspension was poured into 1800 mL of water, and then the mixture was stirred in air for one night, affording a brown CoOOH precipitate. The precipitate was centrifuged, washed with water twice, and then dried at 80 °C in vacuum for 12 h to give nanoplatelet CoOOH. Nanocrystalline $LiCoO_2$ was synthesized through a hydrothermal reaction. CoOOH (184 mg, 2 mmol) was stirred in 30 mL of an aqueous LiOH solution to give a colloidal suspension. The resulting suspension was placed in a stainless steel autoclave, and then the suspension was heated to induce a hydrothermal reaction. After the reaction, the resulting precipitate was collected by centrifugation, washed with water twice, and then dried at 100 °C in a vacuum for 12 h to give nanocrystalline $LiCoO_2$.

Powder X-ray diffraction measurements were carried out on a Bruker D8 Advance using Cu Kα radiation in steps of 0.01° over the 2θ range of 5−80°. The unit cell parameters were calculated by the least-square fitting. Raman spectra were recorded in the backward geometry on a NIHON BUNKO Ventuno spectrometer (NSR-1000DT) at room temperature. Excitation was carried out on the powder samples using the 632.8 nm wavelength line from a He−Ne laser. TEM measurements were carried out on a JEOL JEM-2100F (200 kV). BET surface area with N_2 adsorption was measured on a BEL JAPAN Belsorp plus 18. DC magnetic susceptibility was measured on a Quantum Design MPMS5 SQUID susceptometer with a field of 5000 G. The magnetic susceptibility was corrected for the core diamagnetism estimated from Pascal's constants (-3.50×10^{-5} emu/mol). Li/Co ratio in nanocrystalline $LiCoO_2$ was estimated by inductively coupled plasma atomic emission spectroscopy (ICP-AES) on a RIGAKU CIROS-120.

Each sample (50 mg) was ground with acetylene black (45 mg) and Teflon (5 mg) into a paste and used for the electrochemical measurements. Generally speaking, normal electrodes in commercial Li-ion rechargeable batteries contain only 5% of conductive materials. However, our scope of this paper was focused on the estimation of the high-rate Li-ion intercalation in nanocrystalline $LiCoO_2$. From this viewpoint, we used 45% of the conductive material for bulk $LiCoO_2$ as well as nanocrystalline $LiCoO_2$ in order to improve the conductivity of the electrodes. The high conductivity suppressed some unfavorable problems in the high-rate experiment like an IR drop. Lithium metal was used as the reference and counter electrodes. For the electrolyte, a 1 M $LiClO_4$ EC/DEC solution was used. The cutoff voltages were 4.2 V for charging (deintercalation of Li-ions from $LiCoO_2$) and 3.0 V for discharging (intercalation of Li-ions into $Li_{0.5}CoO_2$). In the high-rate measurement, there was an overpotential problem. Since the voltage for lithium deintercalation at high rates becomes higher than that at 1 C rate, the capacity values obtained from the high-rate charging could not be compared even if we added 45% of the conductive material. In order to evaluate an accurate Li-ion diffusion, charging was carried out at 1 C rate, and only the discharging was performed at a high rate. By using this method, the overpotential problem was avoided, and Li-ion diffusion was accurately measured for each sample.

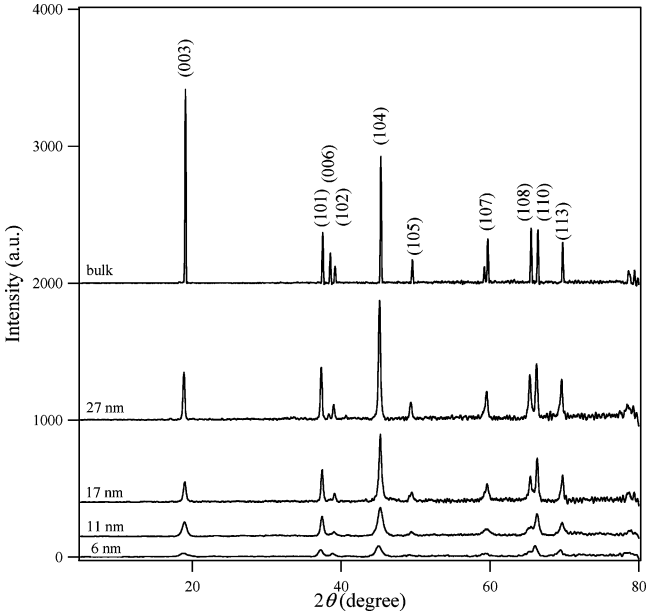

Figure 1. Selected powder X-ray diffraction patterns for nanocrystalline $LiCoO_2$. The diffraction patterns of bulk $LiCoO_2$ are also depicted.

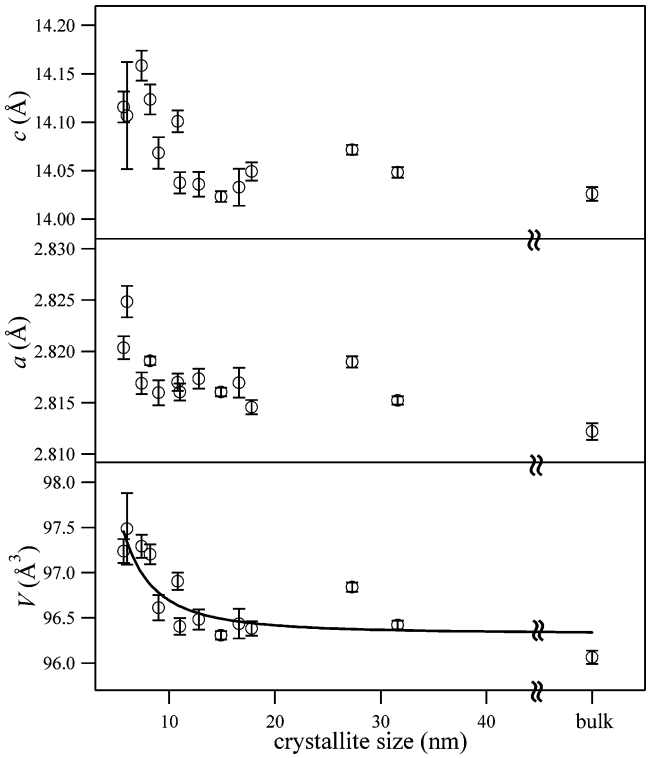

Figure 2. Crystallite size dependence of the unit cell parameters of nanocrystalline $LiCoO_2$.

Results and Discussion

Nanocrystalline $LiCoO_2$ was synthesized through a hydrothermal reaction between CoOOH and an aqueous solution of

(16) Pralong, V.; Delahaye-Vidal, A.; Beaudoin, B.; Gerand, B.; Tarascon, J.-M. *J. Mater. Chem.* **1999**, *9*, 955.

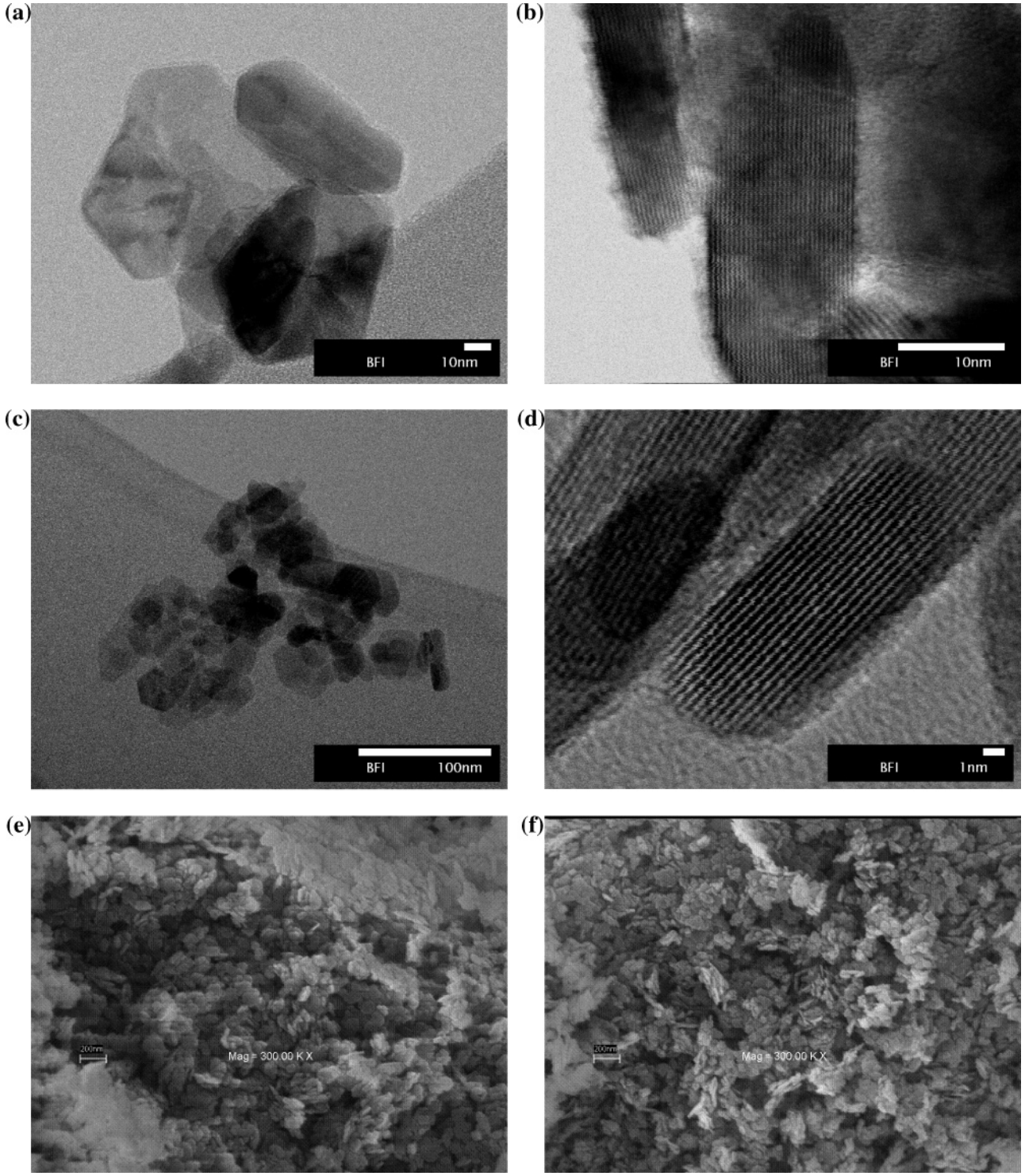

Figure 3. (a, b) TEM images of nanocrystalline $LiCoO_2$ (17 nm). (c, d) TEM images of nanocrystalline $LiCoO_2$ (9 nm). (e) Representative SEM image of nanocrystalline $LiCoO_2$ (17 nm). (f) representative SEM image of nanocrystalline $LiCoO_2$ (9 nm).

LiOH. Although the hydrothermal synthesis has been applied successfully for the synthesis of $LiCoO_2$ by some groups,[12−15] an accurate control of the crystallite size has not been carried out. By varying the reaction temperature, the concentration of the LiOH aqueous solution, and the reaction time, we could accurately control the crystallite size of $LiCoO_2$. Table 1 presents the selected experimental conditions and the resulting products. The hydrothermal reaction with 5 M LiOH solution produced $LiCoO_2$ even after heating at 120 °C for 6 h. On lowering the concentration of LiOH solution, a higher reaction temperature is needed to give $LiCoO_2$.

The resulting products were characterized by using powder X-ray diffraction. Selected powder X-ray diffraction patterns are depicted in Figure 1. All of the peaks corresponded to $LiCoO_2$,[17] which indicates the formation of pure $LiCoO_2$.

(17) Rossen, E.; Reimers, J. N.; Dahn, J. R. *Solid State Ionics* **1993**, *62*, 53.

From the powder X-ray diffraction patterns, we calculated the unit cell parameters for each sample. It should be pointed out that the lattice parameters depend on the crystallite size. The values of *a*, *c*, and *V* are plotted as a function of the crystallite size (*L*) in Figure 2. Compared to bulk $LiCoO_2$ (a = 2.8122(8) Å, c = 14.025(7) Å, and V = 96.06(7) Å^3), the values of *a*, *c*, and *V* with a particle size of 6 nm increased to 2.820(1) Å, 14.12(2) Å, and 97.24(13) Å^3, respectively. The solid line in Figure 2 was fitted to $V(L) = V_0 + k/L^2$, where V_0 = 96.3 Å^3 and k = 36.7 Å^3 · nm^2.

As mentioned in previous reports,[18] stoichiometric $LiCoO_2$ crystallizes in two phases, i.e., a layered α-$NaFeO_2$-type structure (hexagonal, $R\bar{3}m$) and a spinel-type structure (cubic, $Fd\bar{3}m$). Since the powder X-ray diffraction patterns are similar to each other, it is difficult to distinguish between the two structures from the powder X-ray diffraction patterns at a glance. However, the ratio between the lengths of the *a* and *c* axes, *c*/*a*, is known to be a good indicator.[18] While *c*/*a* for a spinel structure is about 4.90, *c*/*a* for a layered structure is about 5.00. As seen in Table 1, *c*/*a* for all products is about 5.00. This indicates that the hydrothermal reaction provided the layered $LiCoO_2$.

The crystallite size of the products was estimated from the (003) and (110) peaks. The (003) peak, which is the stacking direction of the CoO_2 layers, gave crystallite sizes varying from 6 to 32 nm, while the (110) peak, which is the width of the CoO_2 layers, gave larger crystallite sizes from 30 to 60 nm. The estimated crystallite sizes were confirmed by using transmission electron microscopy (TEM). In Figure 3a and b show the TEM images for nanocrystalline $LiCoO_2$, of which the crystallite size was estimated to be 17 nm from the (003) peak and 40 nm from the (110) peak. As seen in Figure 3a, the product had a nanoplatelet morphology, and the width of the CoO_2 layers was about 40 nm. In Figure 3b, the CoO_2 layers are shown. The number of CoO_2 layers was 32, which corresponded to a thickness of 15 nm (0.47 nm × 32 layers). The observed values agreed with the estimated values. In Figures 3, c and d show the TEM images of smaller nanocrystalline $LiCoO_2$ with a thickness of 9 nm from the (003) peak. The 17 CoO_2 layers observed in Figure 3d had a thickness of 8 nm. The observed values agreed with the estimated values by powder X-ray diffraction. In addition, the hexagonal layered platelet morphology strongly indicates that the obtained $LiCoO_2$ is layered $LiCoO_2$.

The observed nanoplatelet morphology also explains the relatively weaker (003) peak than the (104) peak. Generally, as mentioned by Myung et al.,[19] the weak (003) peak indicates the spinel character of $LiCoO_2$. However, since the number of the unit cell along the (003) direction is smaller than that along the (104) direction in the nanoplatelet morphology, the relative intensity of the (003) peak becomes weaker even if $LiCoO_2$ has a layered structure.

Although the TEM images shown in Figure 3 were consistent with the estimated values by powder X-ray diffraction, it is not clear how representative they are. Therefore, the thickness distribution in the TEM images was counted for the compounds with the thickness of 6, 11, and 17 nm, respectively. Figure 4 shows the thickness distribution for each compound. As shown in Figure 4, the compounds with the thicknesses of 6, 11, and 17 nm have a thickness distribution of 6 ± 2, 10 ± 2, and 15 ± 3 nm, respectively. In fact, the representative SEM images of nanocrystalline $LiCoO_2$ with the thickness of 17 nm (Figure 3e) and 9 nm (Figure 3f) show the uniform sizes of the nanoplatelets. Furthermore, the large BET surface areas were determined to be 31.9 m^2/g (the compound with the thickness of 17 nm), 65.3 m^2/g (11 nm), and 78.1 m^2/g (8 nm), respectively. All these results demonstrate that we could control the particle size of $LiCoO_2$ precisely.

As shown in Table 1, the smaller particle was obtained by using higher LiOH concentration, shorter reaction time, or lower reaction temperature. These crystallite size dependencies clearly

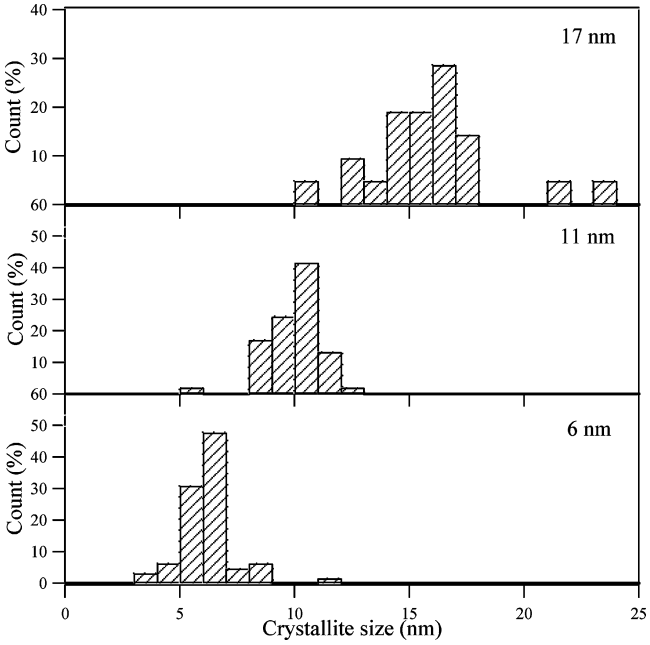

Figure 4. Thickness distributions of nanocrystalline $LiCoO_2$ (6, 11, and 17 nm, respectively).

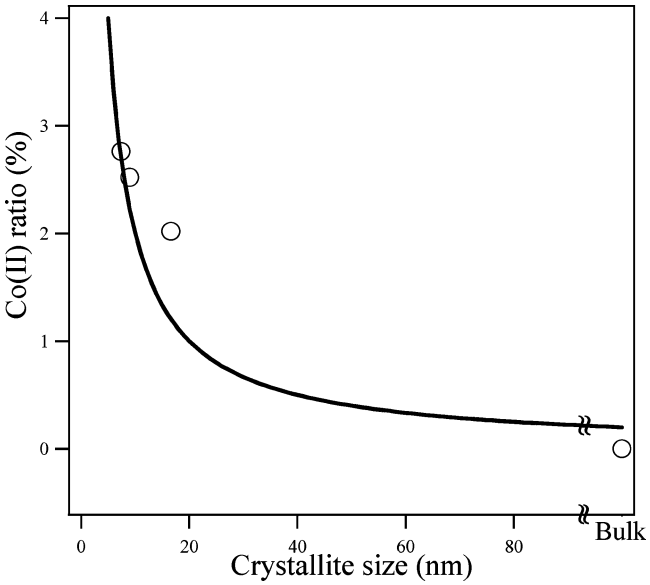

Figure 5. Crystallite size dependence of the Co(II) ion ratio in nanocrystalline $LiCoO_2$. The solid lines are the calculated results (see text).

(18) Gummow, R. J.; Thackeray, M. M.; David, W. I. F.; Hull, S. *Mater. Res. Bull.* **1992**, *27*, 327.
(19) Myung, S. T.; Kumagai, N.; Komaba, S.; Chung, H.-T. *J. Appl. Electrochem.* **2000**, *30*, 1081.

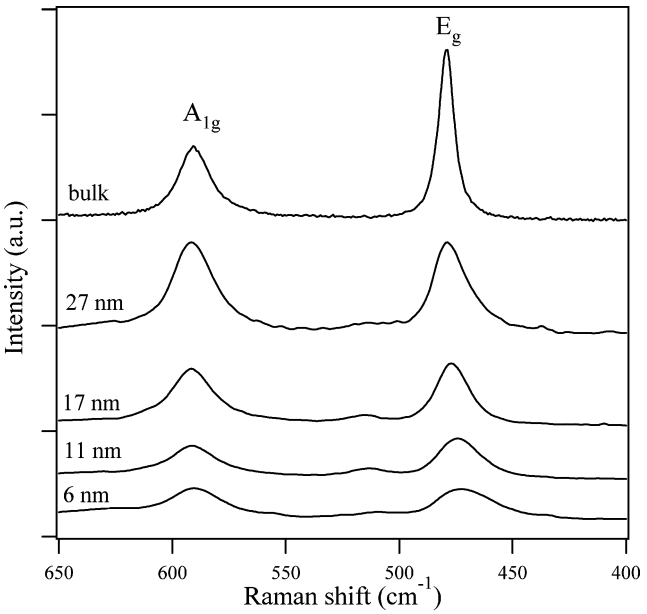

Figure 6. Selected Raman spectra of nanocrystalline $LiCoO_2$. The Raman spectrum of bulk $LiCoO_2$ is shown for comparison.

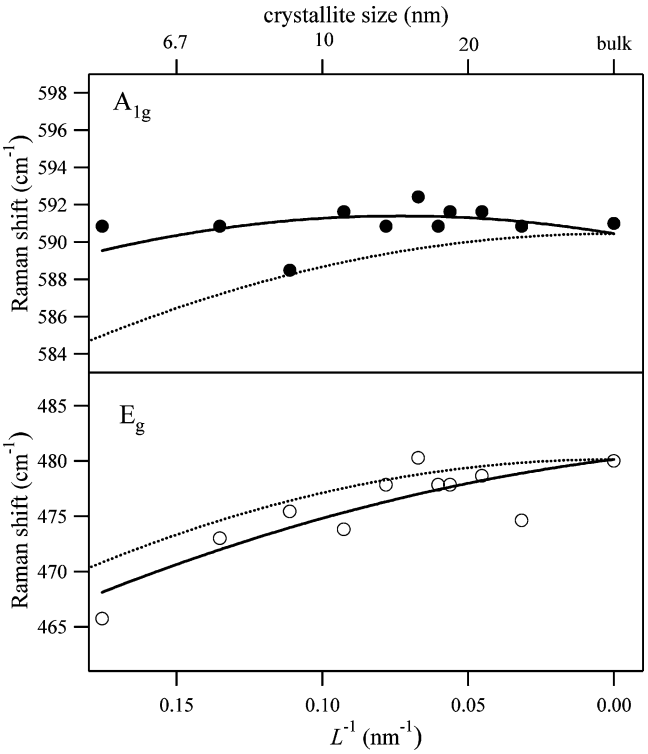

Figure 7. Crystallite size dependence of the Raman peak positions. Dotted lines and solid lines are calculated and fitted results, respectively (see text).

indicate that the reaction mechanism is not a simple ion-exchange process but rather a dissolution−recrystallization process. This mechanism allowed us to control the crystallite size by varying the reaction conditions.

Concerning the lattice expansion in nanocrystalline $LiCoO_2$, similar lattice expansion depending on the particle size has been observed for $BaTiO_3$[20] and CeO_2;[21] however, the mechanism is

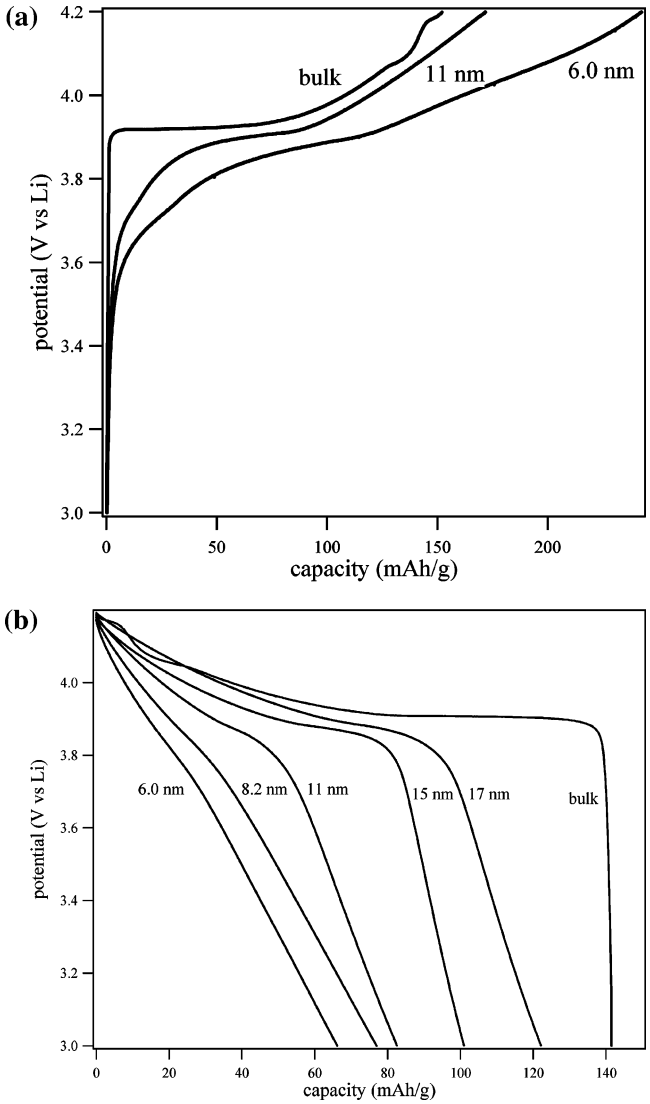

Figure 8. Crystallite size dependence of (a) the first charge curves for $LiCoO_2$ (bulk, 11 and 6 nm), (b) the second discharge curves for $LiCoO_2$ in various size.

still not fully understood. For example, lattice expansion in CeO_2 has been attributed to the electrostatic force reduction accompanied by a charge reduction in the Ce ions, while that in $BaTiO_3$ is ascribed to an unknown change in the Ti−O bonding character.[22] In our case, magnetic susceptibility measurements clarified the origin of the lattice expansion. The magnetic susceptibility of the nanocrystalline $LiCoO_2$ was measured by SQUID. The χT value at room temperature increased with a decrease in the crystallite size. Since the Co(III) ion in $LiCoO_2$ is diamagnetic ($t_{2g}^6e_g^0$), the increase in the χT value was ascribed to high-spin Co(II) ions ($t_{2g}^5e_g^2$, $S = {}^3/_2$). Figure 5 shows the crystallite size dependence on the amount of Co(II) ions. The solid line in Figure 5 indicates the calculated result, assuming that 20% of the cobalt at the surface layer is Co(II) ion. Since the Co(II)−O distance is longer than the Co(III)−O distance due not only to the electrostatic force reduction but also to the antibonding character of the electron occupying the e_g orbital, the existence of Co(II) ion can explain the lattice expansion in nanocrystalline $LiCoO_2$.

(20) Tsunekawa, S.; Ito, S.; Mori, T.; Ishikawa, K.; Li, Z.-Q.; Kawazoe, Y. *Phys. Rev. B* **2000**, *62*, 3065.
(21) Tsunekawa, S.; Sivamohan, R.; Ito, S.; Kasuya, A.; Fukuda, T. *Nanostruct. Mater.* **1999**, *11*, 141.
(22) Tsunekawa, S.; Ito, S.; Mori, T.; Ishikawa, K.; Li, Z.−Q.; Kawazoe, Y. *Phys. Rev. Lett.* **2000**, *85*, 3440.

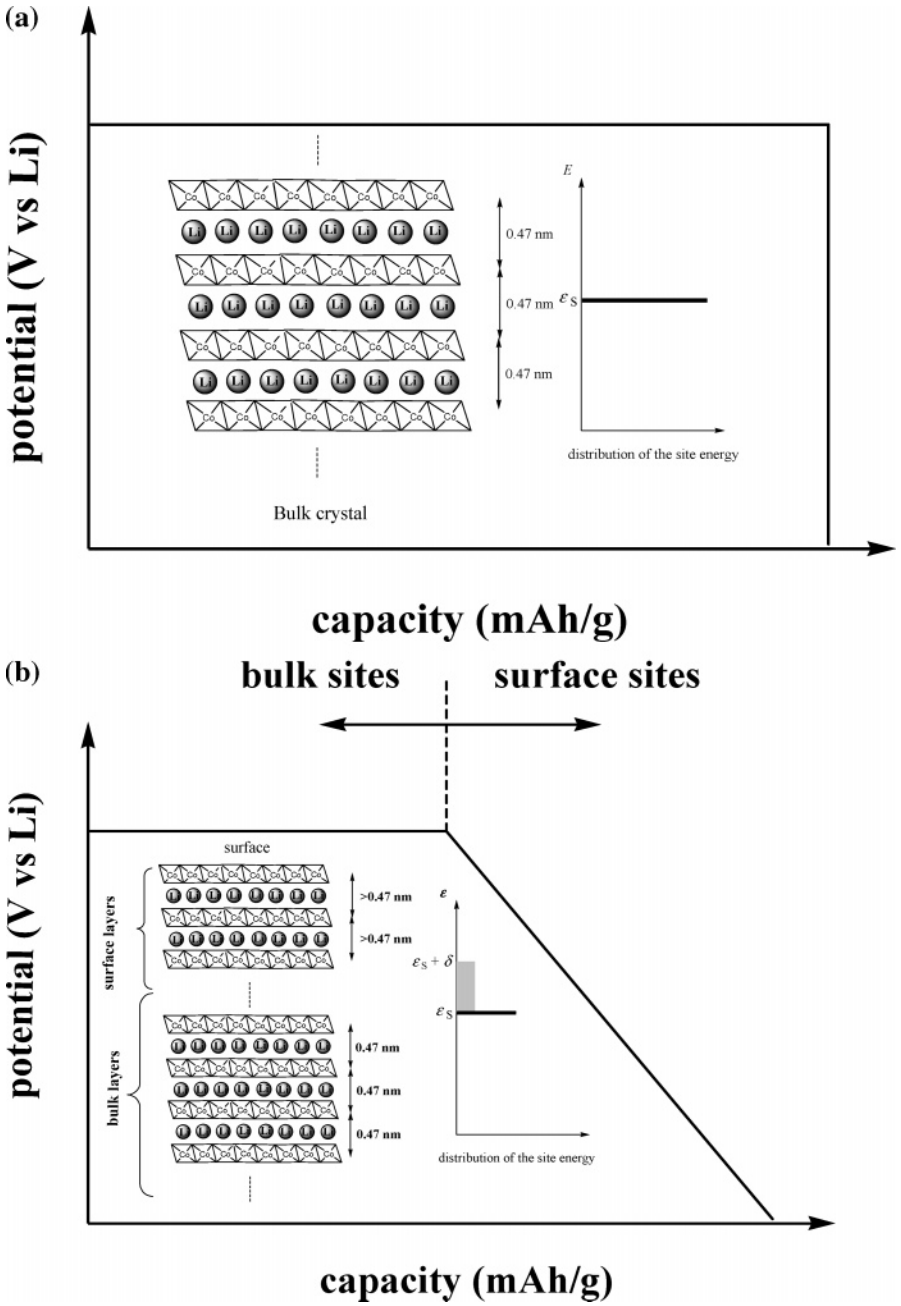

Figure 9. Expected discharge curves for bulk $LiCoO_2$ and nanocrystalline $LiCoO_2$. (a) Expected discharge curve for bulk $LiCoO_2$. (Insets) Ideal structure and the distribution of the site energy. (b) Expected discharge curve for nanocrystalline $LiCoO_2$. (Insets) Disordered structure and the dispersed distribution of the site energy.

The existence of Co(II) ion implies nonstoichiometry like that of $LiCo(II)_\delta Co(III)_{1-\delta}O_{2-\delta}(OH)_\delta$ due to the residual hydroxyl groups of $CoO(OH)$[23] or $Li_{1+\delta}Co(II)_\delta Co(III)_{1-\delta}O_2$ due to excess Li-ions at the surface. On the basis of the ICP measurement, the Li/Co ratio in the compound with the thickness of 8 nm was determined as 1.18. This suggests that nanocrystalline $LiCoO_2$ has the nonstoichiometry of $Li_{1+\delta}Co(II)_\delta Co(III)_{1-\delta}O_2$.

Lattice expansion was also observed by using Raman spectroscopy. Figure 6 shows selected Raman spectra for nanocrystalline $LiCoO_2$ with thicknesses from 6 to 27 nm. Also shown for comparison is the Raman spectrum for commercial $LiCoO_2$. Our samples and commercial $LiCoO_2$ had two strong Raman bands at about 590 cm^{-1} and 480 cm^{-1}. On the basis of factor group analysis on the space group $R\bar{3}m$, these two bands were attributed to the Co−O stretching A_{1g} mode and the O−Co−O bending E_g mode, respectively.[24]

After comparing the Raman spectra more carefully, we determined that there was a systematic change in the peak position of these two Raman bands. Figure 7 shows the relation between the Raman peak positions and the inverse of the crystallite size (L^{-1}), as determined by the (003) peak from powder X-ray diffraction. The top *x*-axis scale in Figure 7 is the crystallite size (L). By using the above value of $V(L)$ ($= 96.3 + 36.7/L^2$) and the previously reported Grüneisen constants

(23) Amatucci, G. G.; Tarascon, J. M.; Larcher, D.; Klein, L. C. *Solid State Ionics* **1996**, *84*, 169.

(24) Inaba, M.; Todzuka, Y.; Yoshida, H.; Grincourt, Y.; Tasaka, A.; Tomida, Y.; Ogumi, Z. *Chem. Lett.* **1995**, *10*, 889.

(0.79 for the A_{1g} mode and 1.15 for the E_g mode),[25] the crystallite size dependencies of the Raman frequency shifts were determined to be $\omega = (590.5 - 177.8)/L^2$ for the A_{1g} mode and $\omega = (480.2 - 210.0)/L^2$ for the E_g mode. The calculated results are shown in Figure 7 as dotted lines. Comparing the calculated results with the experimental data, the observed frequency shift in the A_{1g} mode was much less than that expected from the lattice expansion model. It is clear that the lattice expansion model is not sufficient to explain the crystallite size dependence of the frequency shifts. Therefore, another contribution, i.e., the phonon confinement effect, should be considered.

Generally speaking, the Raman peak position and line width for a nanocrystalline material are affected by phonon confinement. In bulk defect-free crystalline materials, only $q = 0$ phonons are Raman active. Contrary to this, in the case of a nanocrystalline material, q vectors in the range of $\Delta q = 1/L$ (L = crystallite size) become Raman active due to the uncertainty principle, which results in the frequency shift and broadening. The phonon confinement model studied by Richter et al.[26] that was extended by Campbell and Fauchet[27] generates the first-order Raman spectrum from

$$I(\omega) = \int_{BZ} \frac{\exp\left(\frac{-q^2L^2}{8\beta}\right) d^3q}{(\omega - \omega(q))^2 + \left(\frac{\Gamma_0}{2}\right)^2}$$

where the integration is carried out over the Brillouin zone, $\omega(q)$ is the phonon dispersion, β is a confinement parameter, and Γ_0 is the natural line width.

In the phonon confinement model, it is well-known that there is a linear correlation between the Raman frequency shift and $L^{-\alpha}$, where α is a scaling exponent equal to $d/2$ (d = dimensionality).[28] In fact, analyses on three-dimensional materials, such as silicon[26] and gallium arsenide,[29] yielded a scaling factor of about 1.5, whereas analyses on two-dimensional materials, such as graphite[30] and boron nitride,[31] yielded a scaling factor of about 1. Since $LiCoO_2$ is a two-dimensional material, the relationship between the Raman frequency shifts and the inverse of the crystallite size is expected to be linear. Thus, by combining the lattice expansion model and the phonon confinement effect, we fitted the experimental data with $\omega = 590.5 + k_1/L - 177.8/L^2$ for the A_{1g} mode and $\omega = 480.2 + k_2/L - 210.0/L^2$ for the E_g mode. The first term is the Raman frequency for the bulk crystal, the second term is the contribution from the phonon confinement effect, and the last term is the contribution from the lattice expansion effect. The solid lines in Figure 7 represent the least-square fitting results with $k_1 = 26.0$ nm cm^{-1} for the A_{1g} mode and $k_2 = -33.3$ nm cm^{-1} for the E_g mode. Calculated and experimental results for the A_{1g} mode agreed when the phonon confinement effect was included. For the E_g mode, although the lattice expansion model is good, the agreement between the calculated and experimental results was better in this case and is consistent with the lattice expansion.

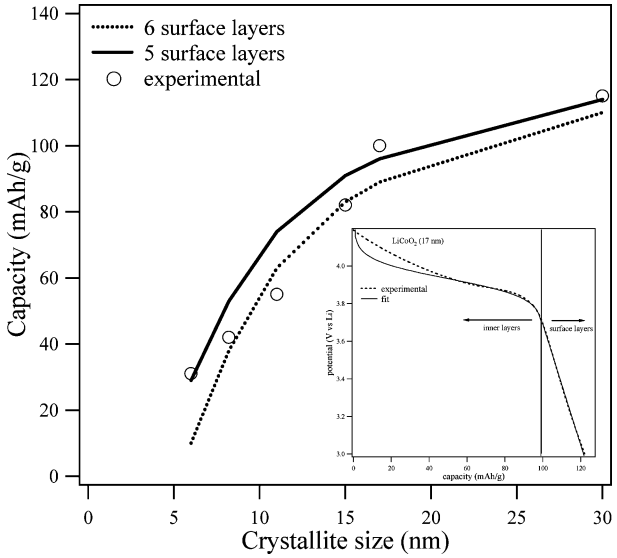

Figure 10. Crystallite size dependence of the capacity for the inner layers. The lines represent the calculated results assuming that five (solid line) or six (dotted line) layers from the surface show a fluctuation in ϵ. (Inset) Typical fitting result (17 nm). The broken line and solid lines denote the experimental results and fitting results, respectively.

In the above discussion, it was shown that the structural nanosize effect occurred in nanocrystalline $LiCoO_2$. It is important to know whether the structural nanosize effect affects the electrochemical properties. In this section, the electrochemical properties of nanocrystalline $LiCoO_2$ are discussed.

Figure 8a shows the first charge curves for three compounds (bulk, 11 and 6 nm) at 1 C rate (deintercalation of Li-ions in 1 h). In general, the first charge curve for the spinel $LiCoO_2$ shows the two charging voltages around 3.4 and 3.8 V, whereas that for the layered $LiCoO_2$ shows the charging voltage above 3.9 V.[32] The observed charging process at lower voltage for nanocrystalline $LiCoO_2$ normally suggests the spinel character of the compounds. However, we should note that we are dealing with nanocrystals, whose structural property is different from that of the bulk one. In fact, TEM, Raman spectroscopy, and powder X-ray diffraction analysis supported the layered character of nanocrystalline $LiCoO_2$. Therefore, the intercalation of Li-ions at lower voltage should suggest the nanosize effect on the electrochemical property of $LiCoO_2$.

Figure 8b shows the discharge curves for various nanocrystalline $LiCoO_2$ (bulk, 6 nm) at 1 C rate. Capacitor behavior became more dominant with decreasing crystallite size, while the plateau region at 3.9 V (the capacity for the inner layers) decreased. Assuming the electric double-layer capacity to be 30 μF/cm^2, the electric double-layer capacity for each compound can be calculated from the BET surface area as 2.6 mA h/g (17 nm), 5.4 mA h/g (11 nm), and 6.4 mA h/g (8 nm), respectively. These values are so small that we can neglect the contribution from the electric double-layer capacitor, and the increasing capacitor behavior is ascribed to the nanosize effect on the intercalation of Li-ions.

(25) Wang, X.; Loa, I.; Kunc, K.; Syassen, K.; Amboage, M. *Phys. Rev. B* **2005**, *72*, 224102.
(26) Richter, H.; Wang, Z. P.; Ley, L. *Solid State Commun.* **1981**, *39*, 625.
(27) Campbell, I. H.; Fauchet, P. M. *Solid State Commun.* **1986**, *58*, 739.
(28) Doss, C. J.; Zallen, R. *Phys. Rev. B* **1993**, *48*, 15626.
(29) Gargouri, M.; Prevot, B.; Schwab, C. *J. Appl. Phys.* **1987**, *62*, 3902.
(30) Nakamura, K.; Fujitsuka, M.; Kitajima, M. *Phys. Rev. B* **1990**, *41*, 12260.
(31) Nemanich, R. J.; Solin, S. A.; Martin, R. M. *Phys. Rev. B* **1981**, *23*, 6348.
(32) Santiago, E. I.; Andrade, A. V. C.; Paiva-Santos, C. O.; Bulhoes, L. O. S. *Solid State Ionics* **2003**, *158*, 91.

Generally speaking, the site energy (ϵ) for the Li-ion intercalation in a bulk crystal is assumed to be constant, $\epsilon = \epsilon_s$, since there is no structural disorder or fluctuation (see inset of Figure 9a). On the basis of a lattice gas model[33] and assuming that the repulsion ($J > 0$) between the nearest Li neighbors is negligible, the expected discharge curve as a function of the capacity is

$$E = \frac{\epsilon_s}{e} - \frac{kT}{e}\ln\left\{\frac{x}{(1-x)}\right\}$$

where x is the lithium site occupancy. Note that this model completely ignores the site occupancy dependence of the site energy, $\epsilon_s(x)$, although there is a phase transition from metal to insulator in varying x. Figure 9a shows the expected discharge curve for a bulk crystal. Under these conditions, intercalation of the Li-ion is expected to take place at a certain voltage, especially at about 3.9 V.

On the other hand, the expected discharge curve for nanocrystalline $LiCoO_2$ was rather complicated. As mentioned above, the lattice expansion in nanocrystalline $LiCoO_2$ was due to the existence of Co(II) ions near the surface layers. Therefore, some of the CoO_2 layers near the surface should have a disordered structure, which induces a fluctuation in ϵ for Li-ion intercalation. Thus, while the ϵ values in the inner layers are equal to that in a bulk crystal (ϵ_s), ϵ near the surface is assumed to be dispersed to a certain extent ($\epsilon_s < \epsilon < \epsilon_s + \delta$). For simplicity, we assumed that ϵ in the nanocrystal was dispersed, as shown in the inset of Figure 9b. On the basis of the lattice gas model and assuming that the lithium site occupancy obeys the Fermi distribution ($x(\epsilon) = [1 + \exp\{(\epsilon - eE)/kT\}]^{-1}$), the expected discharge curve for the surface layers is

$$E = \frac{\epsilon_s}{e} - \frac{kT}{e}\ln\left\{\frac{1-\exp\left(\frac{2\delta x}{kT}\right)}{\exp\left(\frac{2\delta x}{kT}\right)\exp\left(\frac{-\delta}{kT}\right) - \exp\left(\frac{\delta}{kT}\right)}\right\}$$

Figure 9b shows the expected discharge curve for nanocrystalline $LiCoO_2$. Capacitor behavior is expected for the intercalation of the Li-ions into the surface layers. Since the number of surface layers increased with a decrease in the crystallite size, capacitor behavior should become stronger as the crystallite size decreases. This model well explains the experimental results.

We fitted the experimental discharge curves with the expressions from the lattice gas model. The inset of Figure 10 shows a typical fit. By fitting the experimental data with the model, it was possible to distinguish between the capacity of the inner layers and the surface layers. Figure 10 shows the crystallite size dependence on the capacity of the inner layers. The capacity of the inner layers decreased with a decrease in the crystallite size, especially below 15 nm. The solid lines in Figure 10 depict the calculated results, assuming that five or six layers from the surface have the site energy fluctuation; the excellent fit supported this assumption.

As shown in the above experiments, extreme reductions in the crystallite size to less than 15 nm drastically decreased the capacity of $LiCoO_2$. Therefore, from the viewpoint of the relationship between the capacity and the small particle size, crystallite sizes between 15 and 20 nm seem to be appropriate for high-rate charge−discharge measurements. Figure 11a shows the high-rate discharge curve up to 100 C rate for nanocrystalline $LiCoO_2$ (17 nm). At 1 C rate, the capacity was about 120 mA h/g, which was slightly smaller than the ideal capability of $LiCoO_2$ (137 mA h/g). The smaller capacity was explained on the basis of the surface layer effects mentioned previously. Although the capacity tended to decrease with increasing rate, the cell capacity was still 100 mA h/g at 30 C rate (discharge in 2 min), 90 mA h/g at 50 C rate (discharge in 72 s), and 75 mA h/g at 100 C rate (discharge in 36 s).

Figure 11b shows the rate-capability plot for nanocrystalline $LiCoO_2$ (17 nm). The rate-capability plot for bulk $LiCoO_2$

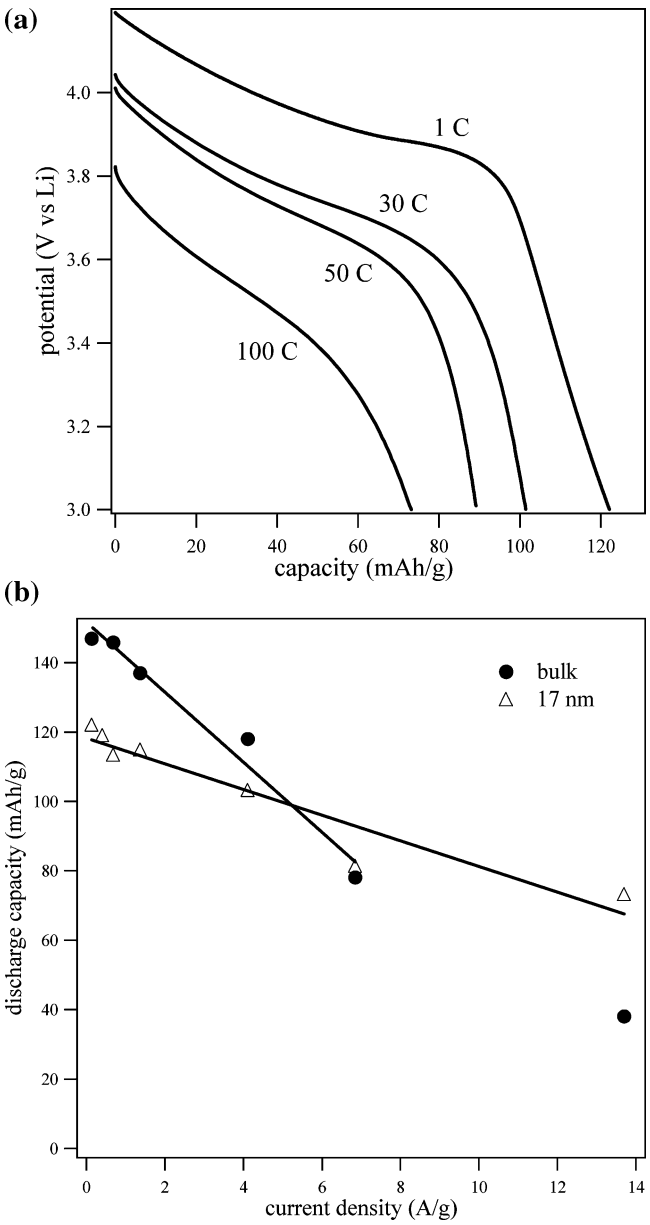

Figure 11. High-rate capability of nanocrystalline $LiCoO_2$. (a) Discharge curves of nanocrystalline $LiCoO_2$ (17 nm) at various discharge rates (1−100 C rate). (b) Rate capability plot for nanocrystalline $LiCoO_2$ (17 nm). The result for bulk $LiCoO_2$ is also shown. The solid lines are fitted results (see text).

(33) Kudo, T.; Hibino, M. *Electrochim. Acta* **1998**, *43*, 781.
(34) Kudo, T.; Hibino, M. *Solid State Ionics* **1996**, *84*, 65.

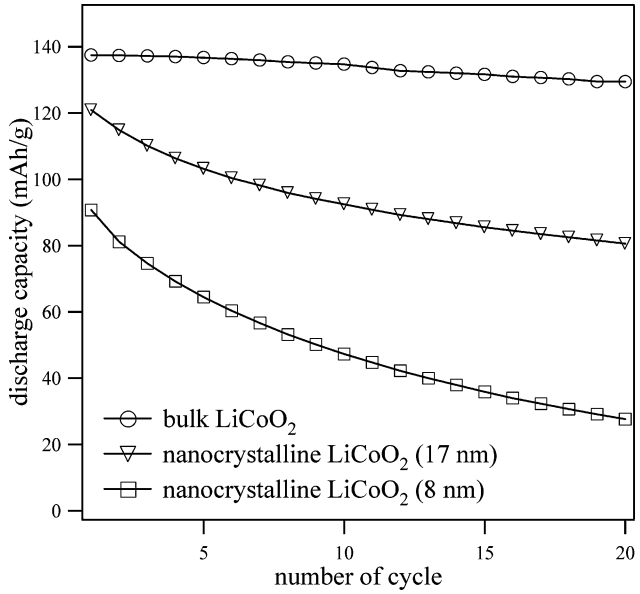

Figure 12. Cyclability of $LiCoO_2$ (bulk, 17 and 8 nm) during 20 cycles at 10 C rate.

is also shown for comparison. Compared to bulk $LiCoO_2$, nanocrystalline $LiCoO_2$ had an excellent rate capability above 30 C rate. While the cell of bulk $LiCoO_2$ at 100 C rate had only 20% of the 1 C rate capability, the cell of nanocrystalline $LiCoO_2$ at 100 C rate retained 65% of the 1 C rate capability.

Furthermore, the analysis on the rate-capability plot in Figure 11b can provide the ratio of the Li-ion diffusion distances for bulk $LiCoO_2$ (d_{bulk}) and nanocrystalline $LiCoO_2$ (d_{17nm}). As mentioned in previous reports,[35−37] a host material with the Li-ion diffusion distance, d, shows a current density (J) dependence of the capacity, Q, as

$$Q = Q_{1C} - \left(\frac{1}{3}\right)\left(\frac{d^2}{D_{Li}}\right)J + \frac{2Jd^2}{D_{Li}\pi^2}\sum_{n=1}^{\infty}\frac{1}{n^2}\exp\left(-\frac{D_{Li}n^2\pi^2Q_{1C}}{d^2J}\right)$$

where Q_{1C} is the capacity at 1 C, and D_{Li} is the Li-ion diffusion coefficient. Note that this model also completely ignores the phase transition of Li_xCoO_2. In the condition of $Q > 0.5Q_{1C}$, the above expression approximates to

$$Q = Q_{1C} - \left(\frac{1}{3}\right)\left(\frac{d^2}{D_{Li}}\right)J$$

Assuming that both compounds have the same D_{Li}, we fitted the rate-capability plot with the expression (solid lines in Figure 11b) and obtained the value of (d_{17nm}/d_{bulk}) as 0.36. This result suggested the positive contribution of the short Li-ion diffusion distance in nanocrystalline $LiCoO_2$ to the high-rate capability. However, the value was higher than the expected value ($d_{17nm}/d_{bulk} = 0.1$) in the assumption of $d_{bulk} = 200$ nm and $d_{17nm} = 20$ nm. This deviation may be due to the other factors such as an IR drop, which is not considered in the model.

Finally, we mention the cyclability of nanocrystalline $LiCoO_2$. Figure 12 shows the discharge capacity of $LiCoO_2$ (bulk, 17 and 8 nm) during 20 cycles at 10 C rate. Compared with bulk $LiCoO_2$, the smaller nanocrystalline $LiCoO_2$ gave the lower cyclability. The large surface area, which easily reacts with the electrolyte at high voltage, should be the main reason for this poor cyclability of nanocrystalline $LiCoO_2$.

Conclusion

In conclusion, we synthesized nanocrystalline $LiCoO_2$ (6−30 nm) and achieved a high-rate capability of lithium ion rechargeable batteries. Nanocrystalline $LiCoO_2$ in various crystallite size was synthesized through the hydrothermal reaction. Varying the reaction conditions strongly affected the crystallite size. This result suggested that the hydrothermal reaction could be a potential synthetic method for other cathode nanoparticles. By using powder X-ray diffraction measurements and Raman spectroscopy, lattice expansion was shown to occur in nanocrystalline $LiCoO_2$. The fluctuation in ϵ induced by the lattice expansion resulted in a decrease in the capacity for the inner bulk layers. The result indicated that extreme size reduction below 15 nm is unfavorable for most applications. Nanocrystalline $LiCoO_2$ with a size of 17 nm had a high-rate capability even at 100 C rate. Although the cyclability and other factors for applications need to be improved, this study is important for nanostructured cathode materials.

Acknowledgment. We thank Mr. Toshio Sasaki (National Institute for Materials Science) for the TEM measurements. This work was supported by the New Energy and Industrial Technology Development Organization Japan, under a grant for Research and Development of Nanodevices for Practical Utilization of Nanotechnology (Nanotech Challenge Project).

JA0681927

(35) Crank, J. C. Mathematics of Diffusion, 2nd ed., Oxford University Press, Oxford, 1975.
(36) Kudo, T.; Ikeda, Y.; Watanabe, T.; Hibino, M.; Miyayama, M.; Abe, H.; Kajita, K. *Solid State Ionics* **2002**, 152−153, 833.
(37) Suzuki, S.; Hibino, M.; Miyayama, M. *J. Power Sources* **2003**, *124*, 513.